JCI The Journal of Clinical Investigation

Optimal bone fracture repair requires 24R,25-dihydroxyvitamin D_3 and its effector molecule FAM57B2

Corine Martineau, … , Glenville Jones, René St-Arnaud

J Clin Invest. 2018;128(8):3546-3557. https://doi.org/10.1172/JCI98093.

Research Article **Bone biology** **Endocrinology**

The biological activity of 24R,25-dihydroxyvitamin D_3 [24R,25$(OH)_2D_3$] remains controversial, but it has been suggested that it contributes to fracture healing. *Cyp24a1*$^{-/-}$ mice, synthesizing no 24R,25$(OH)_2D_3$, show suboptimal endochondral ossification during fracture repair, with smaller callus and reduced stiffness. These defects were corrected by 24R,25$(OH)_2D_3$ treatment, but not by 1,25-dihydroxyvitamin D_3. Microarrays with *Cyp24a1*$^{-/-}$ callus mRNA identified FAM57B2 as a mediator of the 24R,25$(OH)_2D_3$ effect. FAM57B2 produced lactosylceramide (LacCer) upon specific binding of 24R,25$(OH)_2D_3$. *Fam57b* inactivation in chondrocytes (Col2-Cre *Fam57b*$^{fl/fl}$) phenocopied the callus formation defect of *Cyp24a1*$^{-/-}$ mice. LacCer or 24R,25$(OH)_2D_3$ injections restored callus volume, stiffness, and mineralized cartilage area in *Cyp24a1*-null mice, but only LacCer rescued Col2-Cre *Fam57b*$^{fl/fl}$ mice. Gene expression in callus tissue suggested that the 24R,25$(OH)_2D_3$/FAM57B2 cascade affects cartilage maturation. We describe a previously unrecognized pathway influencing endochondral ossification during bone repair through LacCer production upon binding of 24R,25$(OH)_2D_3$ to FAM57B2. Our results identify potential new approaches to ameliorate fracture healing.

Optimal bone fracture repair requires 24R,25-dihydroxyvitamin D_3 and its effector molecule FAM57B2

Corine Martineau,[1] Roy Pascal Naja,[1,2] Abdallah Husseini,[1,3] Bachar Hamade,[1,3] Martin Kaufmann,[4] Omar Akhouayri,[1] Alice Arabian,[1] Glenville Jones,[4] and René St-Arnaud[1,2,3,5,6]

[1]Research Centre, Shriners Hospitals for Children – Canada, Montreal, Quebec, Canada. [2]Department of Human Genetics, and [3]Department of Surgery, McGill University, Montreal, Quebec, Canada. [4]Department of Biomedical and Molecular Sciences, Queen's University, Kingston, Ontario, Canada. [5]Department of Medicine, McGill University, Montreal, Quebec, Canada. [6]Research Institute of the McGill University Health Centre, Montreal, Quebec, Canada.

The biological activity of 24R,25-dihydroxyvitamin D_3 [24R,25$(OH)_2D_3$] remains controversial, but it has been suggested that it contributes to fracture healing. *Cyp24a1*$^{-/-}$ mice, synthesizing no 24R,25$(OH)_2D_3$, show suboptimal endochondral ossification during fracture repair, with smaller callus and reduced stiffness. These defects were corrected by 24R,25$(OH)_2D_3$ treatment, but not by 1,25-dihydroxyvitamin D_3. Microarrays with *Cyp24a1*$^{-/-}$ callus mRNA identified FAM57B2 as a mediator of the 24R,25$(OH)_2D_3$ effect. FAM57B2 produced lactosylceramide (LacCer) upon specific binding of 24R,25$(OH)_2D_3$. *Fam57b* inactivation in chondrocytes (Col2-Cre *Fam57b*$^{fl/fl}$) phenocopied the callus formation defect of *Cyp24a1*$^{-/-}$ mice. LacCer or 24R,25$(OH)_2D_3$ injections restored callus volume, stiffness, and mineralized cartilage area in *Cyp24a1*-null mice, but only LacCer rescued Col2-Cre *Fam57b*$^{fl/fl}$ mice. Gene expression in callus tissue suggested that the 24R,25$(OH)_2D_3$/FAM57B2 cascade affects cartilage maturation. We describe a previously unrecognized pathway influencing endochondral ossification during bone repair through LacCer production upon binding of 24R,25$(OH)_2D_3$ to FAM57B2. Our results identify potential new approaches to ameliorate fracture healing.

Introduction

Vitamin D_3 must be metabolized twice to function as a key regulator of mineral ion homeostasis. In the liver, it is hydroxylated at carbon 25, and in the kidney, it is hydroxylated at position 1 to produce 1,25$(OH)_2D_3$, the hormonal form of vitamin D_3 (1). Upon reaching its target tissues, 1,25$(OH)_2D_3$ binds to its specific receptor, the vitamin D receptor (VDR), to regulate the transcription of vitamin D_3 target genes responsible for carrying out the physiological actions of 1,25$(OH)_2D_3$: mineral homeostasis, skeletal homeostasis, and cellular differentiation (2). Among several target genes, the 1,25$(OH)_2D_3$ hormone induces in target cells the expression of the gene encoding the key effector of its catabolic breakdown: 25-hydroxyvitamin D-24-hydroxylase (*Cyp24a1*) (3). This ensures attenuation of the 1,25$(OH)_2D_3$ biological signal inside target cells and helps regulate vitamin D_3 homeostasis.

CYP24A1 catalyzes the addition of a hydroxyl group on carbon 24 of 1,25$(OH)_2D_3$ (4). This initiates the 24-oxidation pathway leading to 1,25$(OH)_2D_3$ catabolism (3). The 25$(OH)D_3$ metabolite also serves as a substrate for the CYP24A1 enzyme, leading to the production of 24R,25$(OH)_2D_3$ (4, 5). The bioactivity of 24R,25$(OH)_2D_3$ remains controversial. It has been proposed that it might contribute to fracture repair (6–8), but limited information is available on this putative function of the metabolite.

Indirect (secondary) bone healing is the most common fracture repair mechanism, since it does not require rigidly stable conditions (9). This process begins with an acute inflammatory response at the fracture site, where immune and precursor cells are recruited. The fracture gap is then bridged by fibrocartilaginous callus tissue subsequently mineralized through endochondral and intramembranous ossification. Finally, the mineralized callus is progressively remodeled into lamellar bone (9).

The idea that 24R,25$(OH)_2D_3$ contributes to bone healing stems from the observation that its circulating levels increase during fracture repair in chickens as a result of an increase in CYP24A1 activity (8). When the effect of various vitamin D_3 metabolites on the mechanical properties of healed bones was tested, treatment with 24R,25$(OH)_2D_3$ was necessary to achieve optimal healing (6). These results indicate that 24R,25$(OH)_2D_3$ plays an essential role as a vitamin D metabolite important for fracture repair. The mechanism of action has remained elusive, although studies have suggested the presence of a binding activity for 24R,25$(OH)_2D_3$ in membrane fractions from chicken tibial fracture–healing callus (7, 10).

We took advantage of the previously generated *Cyp24a1*-null mice (11) to examine the putative role of 24R,25$(OH)_2D_3$ and its mechanism of action in mammalian fracture repair. We have measured a significant, reproducible impairment in callus formation during fracture repair in *Cyp24a1*-null mice. The callus formation defect was corrected by exogenous administration of 24R,25$(OH)_2D_3$, but not by treatment with 1,25$(OH)_2D_3$. Using *Cyp24a1*-null callus tissue, we identified and cloned

Conflict of interest: The authors have declared that no conflict of interest exists.
Submitted: October 16, 2017; **Accepted:** May 8, 2018.
Reference information: *J Clin Invest*. 2018;128(8):3546–3557.
https://doi.org/10.1172/JCI98093.

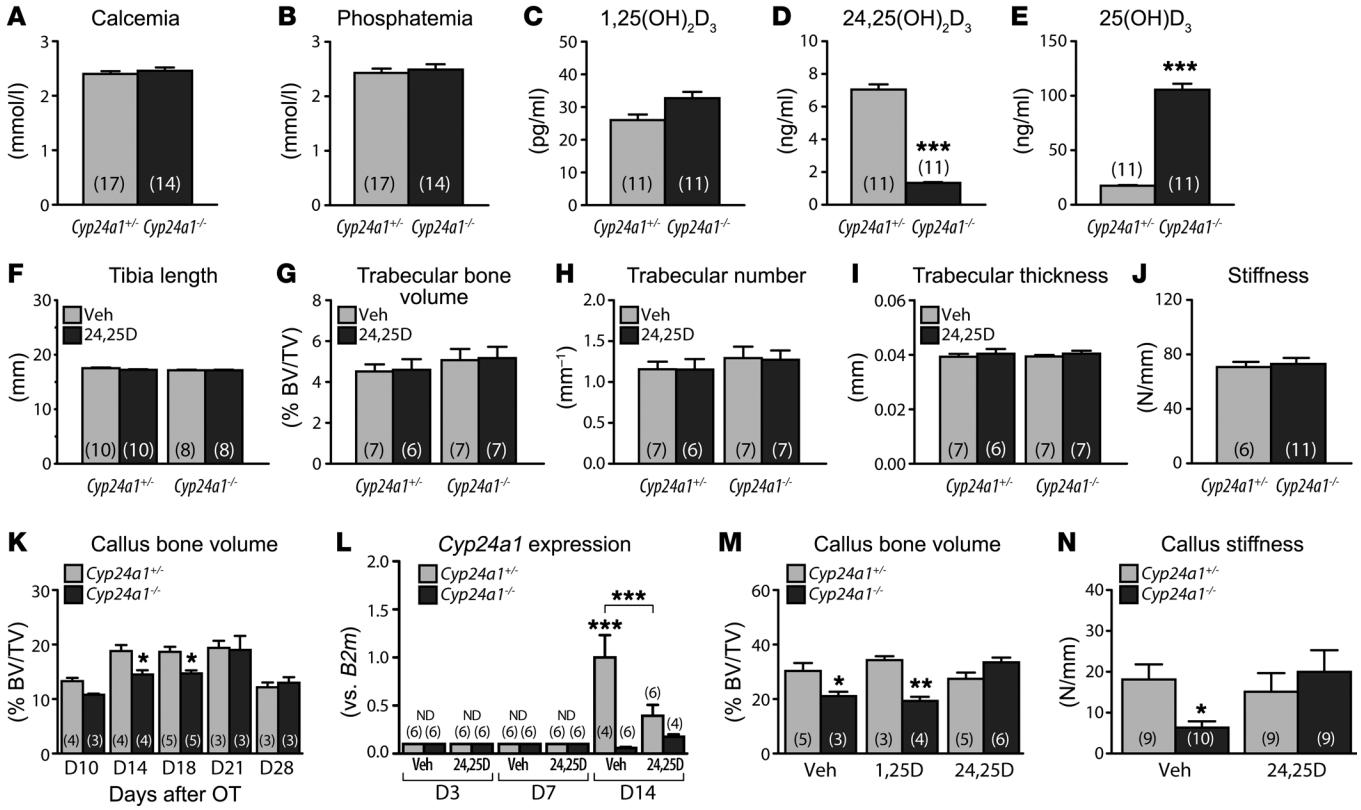

Figure 1. Bone fracture phenotype of *Cyp24a1*-null mice. (**A**–**E**) Blood biochemistry in control and *Cyp24a1*-mutant mice. (**A**) Circulating calcium levels. $P = 0.4568$, by 2-tailed t test. (**B**) Phosphatemia. $P = 0.2429$, by 2-tailed t test. (**C**–**E**) Vitamin D metabolites. ***$P < 0.001$, by 2-tailed t test. (**F**–**I**) Static morphometry in untreated and 24R,25$(OH)_2D_3$-supplemented control and mutant *Cyp24a1* mice. Bone length (**F**), trabecular bone volume (**G**), trabecular number (**H**), and trabecular thickness (**I**) were assessed by micro-CT. $P > 0.05$, by 2-way ANOVA followed by Bonferroni's post test for **F**–**I**. (**J**) Bone stiffness was calculated from the 3PBT. $P = 0.7420$, by 2-tailed t test. (**K**) Fracture repair callus volume following intramedullary rod–stabilized osteotomy (OT). *P < <0.05, by 2-way ANOVA followed by Bonferroni's post test. (**L**) *Cyp24a1* expression in callus tissue from control and *Cyp24a1*-null mice, with or without 24R,25$(OH)_2D_3$ rescue. ND, not detectable. ***$P < 0.001$, by 2-way ANOVA followed by Bonferroni's post test. (**M**) Rescue treatment with vitamin D_3 metabolites of osteotomies immobilized by external fixator. *$P < 0.05$ and **$P < 0.01$, by 2-way ANOVA followed by Bonferroni's post test. (**N**) Rescue of biomechanical properties by 24R,25$(OH)_2D_3$ administration. *$P < 0.05$, by 2-way ANOVA followed by Bonferroni's post test. Data represent the mean ± SEM. The number of animals per group is indicated in parentheses. D, day; 24,25D, 24R,25$(OH)_2D_3$; 1,25D, 1,25$(OH)_2D_3$; Veh, vehicle.

Fam57b2, encoding a transmembrane protein that interacts with 24R,25$(OH)_2D_3$ in a specific, saturable manner. FAM57B2 produced lactosylceramide (LacCer), a neutral glycosphingolipid abundant in articular cartilage (12), upon 24R,25$(OH)_2D_3$ binding in vitro. Our results describe a physiological pathway involving 24R,25$(OH)_2D_3$-dependent, FAM57B2-mediated LacCer synthesis for optimal bone fracture repair.

Results

Systemic deficiency in 24R,25$(OH)_2D_3$ impairs bone fracture repair in mice. The survival and normal skeletogenesis of *Cyp24a1*-null mice born from heterozygous females (11) allowed us to study bone healing in these animals. Since heterozygous *Cyp24a1*$^{+/-}$ animals exhibit a WT phenotype (ref 11; see also Supplemental Table 1 and Supplemental Figures 1 and 2; supplemental material available online with this article; https://doi.org/10.1172/JCI98093DS1), we used them as controls. Surviving *Cyp24a1*-null mice were normocalcemic and normophosphatemic (Figure 1, A and B), with circulating levels of 1,25$(OH)_2D_3$ comparable to those of controls (Figure 1C and Supplemental Figure 1E). Serum concentrations of 24R,25$(OH)_2D_3$ were undetectable (Figure 1D, lower detection limit of the assay), and circulating 25$(OH)D_3$ was elevated (Figure 1E). Neither *Cyp24a1* deletion nor exogenous 24R,25$(OH)_2D_3$ injections in control or *Cyp24a1*-null mice had any effect on basal bone constitution, as tibia length (Figure 1F), trabecular structure (volume, number, and thickness) (Figures 1, G–I), and tibia stiffness (Figure 1J) were not altered. A bone fracture–healing time course in 12-week-old *Cyp24a1*-null mice revealed a significant, reproducible reduction in callus volume compared with that of control littermates on post-osteotomy days 14 and 18, which caught up at later time points (Figure 1K). This impairment in callus formation was observed whether the osteotomized bone was immobilized via intramedullary rodding (Figure 1K) or with an external fixator (Figure 1M, vehicle). All further experiments therefore took place on day 14 or day 18. Since local production of 24R,25$(OH)_2D_3$ was reported in chicken callus, we monitored *Cyp24a1* expression in callus tissue of control and null mice. We detected *Cyp24a1* expression in control callus tissue starting on day 14 (Figure 1L). Systemic injection of 24R,25$(OH)_2D_3$ decreased *Cyp24a1* expression (Figure 1L) and restored mineral-

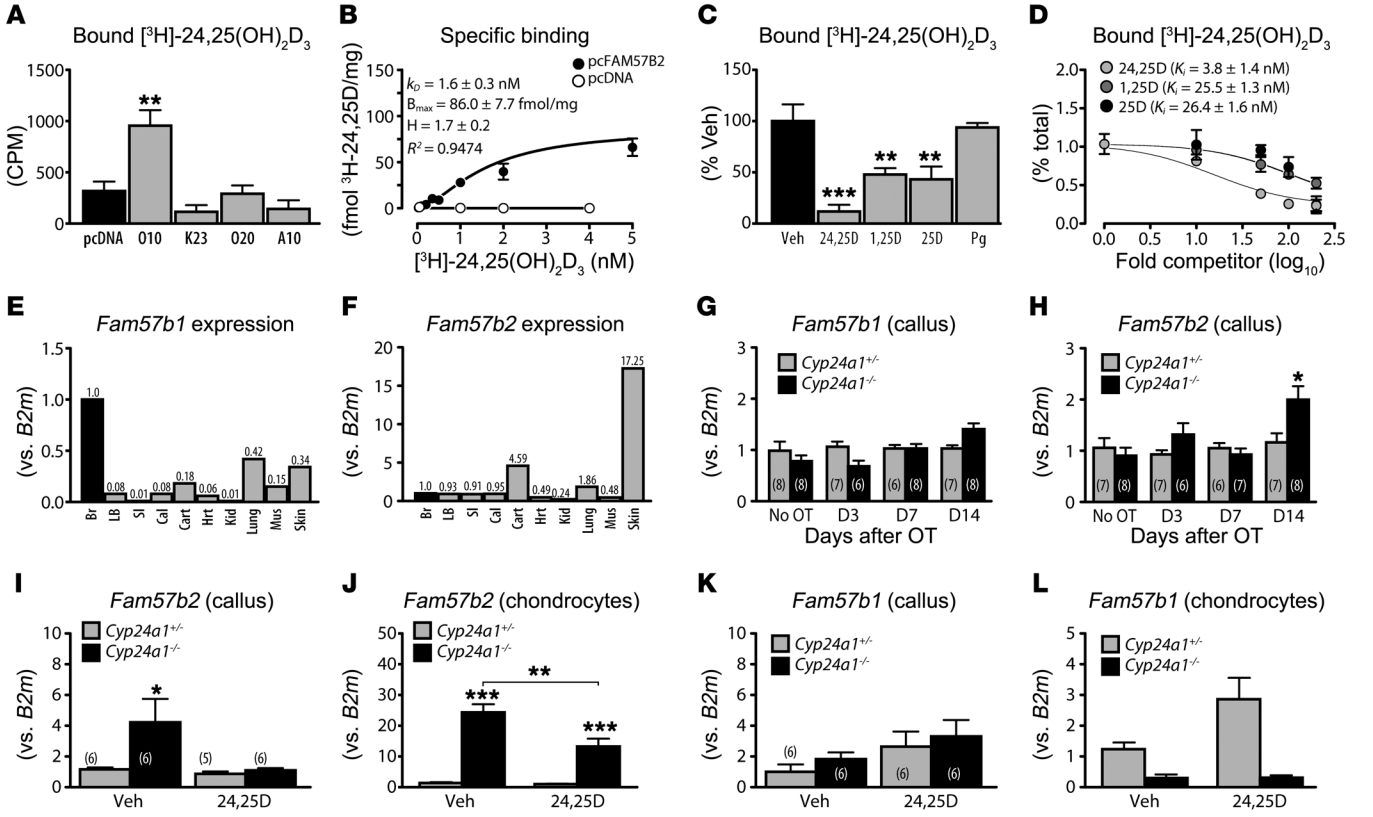

Figure 2. Cloning and characterization of *Fam57b2* from *Cyp24a1*-null callus tissue. (**A**) Binding of [^{3}H]- 24R,25(OH)$_2$D$_3$ to cDNAs identified by microarray analyses. $^{**}P < 0.01$, by 1-way ANOVA followed by Dunnett's post test ($n = 3$). (**B**) Saturation binding analysis (1-site–specific binding with Hill slope; $n = 3$). (**C** and **D**) Binding competition analysis. $^{**}P < 0.01$ and $^{***}P < 0.001$, by 1-way ANOVA followed by Dunnett's post test; 1-site fit K_i ($n = 3$). Pg, progesterone. (**E** and **F**) *Fam57b* isoform expression in tissues. Relative expression levels were determined by reverse transcription quantitative PCR (RT-qPCR) and normalized to *B2m*. Expression in brain (Br) was arbitrarily assigned a value of 1. LB, long bones; SI, small intestine; Cal, calvaria; Cart, cartilage; Hrt, heart; Kid, kidney; Mus, skeletal muscle. Relative expression is indicated by numerals above each bar. (**G** and **H**) *Fam57b* isoform expression in fracture callus. Relative expression levels were determined at intervals by RT-qPCR and normalized to *B2m*; expression in contralateral tibia (No OT) was arbitrarily assigned a value of 1. $^*P < 0.05$, by 2-way ANOVA followed by Bonferroni's post test. (**I**–**L**) Expression of *Fam57b* isoforms following 24R,25(OH)$_2$D$_3$ treatment in callus (**I** and **K**) or primary cultures of chondrocytes (**J** and **L**). $^*P < 0.05$, $^{**}P < 0.01$, and $^{***}P < 0.001$, by 2-way ANOVA followed by Bonferroni's post test ($n = 6$). The number of animals per group is indicated in parentheses.

ized callus volume (Figure 1M) and mechanical properties (Figure 1N). We found that administration of 1,25(OH)$_2$D$_3$ did not restore mineralized callus volume (Figure 1M).

Fam57b identification from callus tissue. Gene expression monitoring with microarrays using RNA from day 14 callus tissue of control or *Cyp24a1*-null mice was performed to identify potential effector molecules of the 24R,25(OH)$_2$D$_3$ signal. We postulated that in the absence of a putative 24R,25(OH)$_2$D$_3$ negative feedback loop, the gene encoding the effector molecule may be overexpressed in the repair callus from *Cyp24a1*$^{-/-}$ animals. Since previous studies suggested the presence of a membrane receptor for 24R,25(OH)$_2$D$_3$ in chicken tibial fracture callus (7, 10), we added the selection criterion of membrane-associated proteins with no annotated function (at the time the assay was performed). The microarray analysis identified 4 genes that were selectively upregulated in null tissue and met the other selection criteria: RIKEN clones 1500002O20, 2310046K23, 1500016O10, and 1110020A10 (Supplemental Table 2). Only clone 1500016O10 was shown to bind tritiated 24R,25(OH)$_2$D$_3$ (Figure 2A). Membrane extracts from 1500016O10-overexpressing COS7 cells bound [^{3}H]-24R,25(OH)$_2$D$_3$ in a saturable manner, with a K_D in the range of 1.6 ± 0.3 nM and a Hill coefficient (13) of 1.7 ± 0.2 (Figure 2B). Excess unlabeled 24R,25(OH)$_2$D$_3$ efficiently competed with the tritiated ligand, while 1,25(OH)$_2$D$_3$ and 25(OH)D$_3$ had lower affinity (Figure 2C). Their K_i were approximately 7-fold higher than that of 24R,25(OH)$_2$D$_3$ (Figure 2D). Progesterone did not compete for binding of [^{3}H]-24,25(OH)$_2$D$_3$ (Figure 2C).

Basic Local Alignment Search Tool (BLAST) screening of the 150006O10 sequence against the *Mus musculus* genome identified *Fam57b* as the only match (Supplemental Figure 3A). This gene encodes 3 protein isoforms, differing by the first 50 amino acid residues of their N-termini (Supplemental Figure 3B). We ran an isoform-specific expression panel in various tissues and found that *Fam57b1* was preferentially expressed in the brain (Figure 2E), while *Fam57b2* was most prominent in cartilage and skin, with levels in lung somewhat higher than those in the brain (Figure 2F). Isoform 3 was reported to be preferentially expressed in testis (14) and was not further investigated. *Fam57b2* expression was upregulated in *Cyp24a1*-null lung tissue but not in skin (Supplemental Figure 4). A time-course analysis of the expression of *Fam57b* isoforms in callus tissue from *Cyp24a1*-null mice and control littermates showed

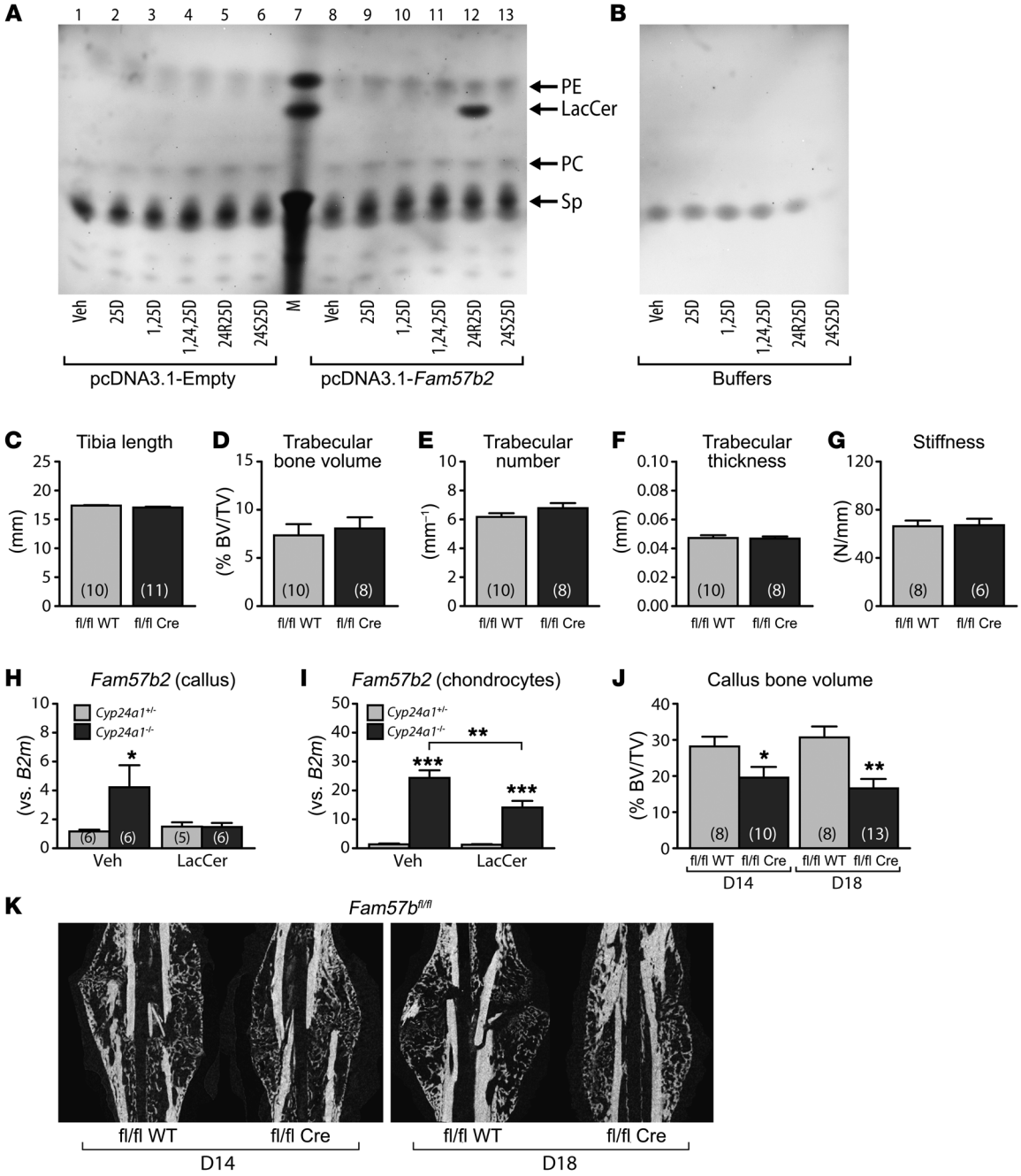

Figure 3. FAM57B2 functional characterization. (**A** and **B**) Ceramide synthase assay. Lysates from HEK293 cells transfected with *Fam57b2* or empty vector (**A**) were used in enzyme assays. Products were separated by TLC as described in Methods. Arrows indicate lipid standards. Results are representative of 3 independent experiments. 25D, 25(OH)D_3; 24R25D, 24R,25$(OH)_2D_3$; 24S25D, 24S,25$(OH)_2D_3$; 1,25D, 1,25$(OH)_2D_3$; 1,24,25D, 1,24,25$(OH)_3D_3$; M, lipid markers: PE, LacCer, PC, and Sp. (**C**–**F**) Static morphometry in control (fl/fl WT) and chondrocyte-specific mutant (fl/fl Cre) *Fam57b*-floxed mice. Bone length (**C**) and trabecular bone volume (**D**), number (**E**), and thickness (**F**) were assessed by micro-CT. $P > 0.05$, by 2-tailed *t* test for **C**–**F**. (**G**) Bone stiffness was calculated from the 3PBT. $P > 0.05$, by 2-tailed *t* test. (**H**) *Fam57b2* expression in day-18 fracture callus from control or *Cyp24a1*$^{-/-}$ mice supplemented or not with 50 μg/kg daily C18-LacCer. $^*P < 0.05$, by 2-way ANOVA followed by Bonferroni's post test. (**I**) *Fam57b2* expression in primary chondrocytes from control or *Cyp24a1*$^{-/-}$ mice, with or without a 24-hour exposure to 1 μM LacCer. $^{**}P < 0.01$ and $^{***}P < 0.001$, by 2-way ANOVA followed by Bonferroni's post test ($n = 6$). (**J**) Callus volume quantification was determined by micro-CT. $^*P < 0.05$ and $^{**}P < 0.01$, by 2-way ANOVA followed by Bonferroni's post test. (**K**) X-ray projections of callus of chondrocyte-specific *Fam57b*-deficient mice on day 14 and day 18 after osteotomy. fl/fl WT, control *Fam57b* mice; fl/fl Cre, chondrocyte-specific *Fam57b*-deficient mice. The number of animals per group is indicated in parentheses.

that isoform 1 remained expressed at low levels and was not modulated during fracture repair (Figure 2G). In contrast, isoform 2 was found to be significantly upregulated on post-osteotomy day 14 in *Cyp24a1*-null callus tissue (Figure 2H). Treatment with 24R,25$(OH)_2D_3$ reduced *Fam57b2* expression in *Cyp24a1*-deficient fracture callus at day 18 (Figure 2I) as well as in primary cultures of chondrocytes (Figure 2J), supporting the retroinhibition feedback mechanism postulated as a criterion for microarray target selec-

tion. We found that supplementation with 24R,25$(OH)_2D_3$ had no impact on the relative expression levels of *Fam57b1* in either genotype, whether in vivo (Figure 2K) or in vitro (Figure 2L).

In vitro characterization of FAM57B2 protein. In addition to transmembrane motifs, FAM57B2 contains a domain related to acyl-CoA–dependent ceramide synthase, and overexpression of FAM57B2 was reported to increase ceramide production in adipocytes (14). We adapted this assay to challenge FAM57B2 (from transfected HEK293 cells) with vitamin D_3 metabolites to determine whether 24R,25$(OH)_2D_3$ binding could modulate FAM57B2 enzymatic activity. Because this protocol requires the presence of BSA, which reduces metabolite availability, we increased the effective dose of 24R,25$(OH)_2D_3$ to 1 μM, despite the nM-range K_D. Moreover, the substrate and cofactor concentrations are set in the μM range for the assay (14). Cells were grown in vitamin D_3–depleted serum for the preparation of lysates used in the enzyme assay. We observed 24R,25$(OH)_2D_3$-dependent production of LacCer [*β*-D-galactosyl-(1-4)-*β*-D-glucosyl-(1-1′)-ceramide] by FAM57B2 (Figure 3A, lane 12). The allosteric modulation of FAM57B2 enzymatic activity was specific to the natural epimer of the 24-hydroxylated metabolite 24R,25$(OH)_2D_3$ (15, 16), as preincubation with either 25$(OH)D_3$; 1,25$(OH)_2D_3$; 1,24,25$(OH)_3D_3$; or the non-natural epimer 24S,25$(OH)_2D_3$ (15, 16) was without effect (Figure 3A, lanes 9–11 and lane 13, respectively). Cell lysates from vector-transfected cells did not produce LacCer (Figure 3A, lanes 1–6), and we detected no contaminants in the reaction buffers (Figure 3B).

Involvement of FAM57B2 in fracture repair in vivo. We generated a mouse strain in which the *Fam57b* gene can be specifically inactivated in selected tissues. Removal of the floxed exon 6 introduced a frameshift and produced a null allele (Supplemental Figure 5A). We bred *Fam57b*-floxed mice with Col2-Cre–transgenic mice (17) to achieve chondrocyte-specific gene inactivation (Supplemental Figure 5B). This was confirmed by immunofluorescence staining of growth plate sections from Col2-Cre *Fam57b*$^{fl/fl}$ mice with an anti-FAM57B antibody (Supplemental Figure 5C). Since *Fam57b2* is the main isoform expressed in chondrocytes (Figure 2, E and F), this strategy allowed for evaluation of the putative role of FAM57B2 in endochondral ossification during fracture repair. First, we verified that tibia length (Figure 3C), trabecular structure (volume, number, and thickness) (Figure 3, D–F), and tibia stiffness (Figure 3G) remained unaffected by the chondrocyte-specific gene deletion under basal conditions. The fact that *Fam57b2* expression was normalized by LacCer treatment in *Cyp24a1*$^{-/-}$ callus tissue (Figure 3H) and primary chondrocytes (Figure 3I) suggests some type of feedback mechanism. If FAM57B2 is a physiological effector of the 24R,25$(OH)_2D_3$ signal, the model predicts that chondrocyte-specific inactivation of *Fam57b* will replicate the impaired callus formation phenotype of *Cyp24a1*-null mice that cannot generate the 24R,25$(OH)_2D_3$ ligand. Indeed, Col2-Cre *Fam57b*$^{fl/fl}$–mutant mice phenocopied the lower callus volume observed in the *Cyp24a1*-null mouse on days 14 and 18 (Figure 3, J and K). There were no phenotypic differences among any of the control genotypes (*Fam57b*$^{+/fl}$, *Fam57b*$^{fl/fl}$, and Col2-Cre *Fam57b*$^{+/fl}$) (Supplemental Figure 5, D and E), so the mutant phenotype was compared with that of the *Fam57b*$^{fl/fl}$ littermates. We observed the phenotype in both female (Figure 3, J and K) and male (Supplemental Figure 6) mutant mice.

In vivo rescue experiments. To confirm the involvement of LacCer in bone fracture repair, *Cyp24a1*-null and chondrocyte-specific *Fam57b*-deleted mice were injected subcutaneously with this lipid after osteotomy. Computer-assisted microtomography (micro-CT) analyses revealed normalization of callus volume by LacCer supplementation in both mouse strains (Figure 4, A and E). Callus stiffness was also rescued by this treatment (Figure 4, B and F). Histological measurements confirmed normalization of the lower mineralized cartilage proportion in both mutant mouse strains by LacCer (Figure 4, C, D, G, and H). However, supplementation with 24R,25$(OH)_2D_3$ did not rescue the fracture-healing impairment in Col2-Cre *Fam57b*$^{fl/fl}$ mice, as callus volume (Figure 4I), stiffness (Figure 4J), and mineralized cartilage (Figure 4, K and L) remained diminished. Taken together, our data show that CYP24A1 and FAM57B2 form part of a common pathway to optimize bone fracture repair, with LacCer production by FAM57B2 acting downstream of the 24R,25$(OH)_2D_3$ signal.

Monitoring of chondrogenic marker expression in callus. Our data suggest that healing was impaired during the endochondral phase of fracture repair in *Cyp24a1*-null and chondrocyte-specific *Fam57b*-deleted mice. We thus monitored the expression of markers of cartilage maturation in calluses from control and mutant littermates during the rescue treatment. Of the genes assessed, collagen type II α 1 chain (*Col2a1*) and aggrecan (*Acan*) were both upregulated by either 24R,25$(OH)_2D_3$ or LacCer treatment in the *Cyp24a1*-null calluses (Figure 5, A and B), but as expected, their expression remained unaffected by 24R,25$(OH)_2D_3$ treatment in Col2-Cre *Fam57b*$^{fl/fl}$ calluses (Figure 5, C and D). Interestingly, the observed effects were more pronounced in the mutant mice, which may be due to the high levels of 24R,25$(OH)_2D_3$ reached during treatment (Supplemental Figure 7B). We observed similar trends for the effect of treatments on the expression of cartilage oligomeric matrix protein (*Comp*) (Figure 5, E and G), hyaluronan and proteoglycan link protein 1 (*Hapln1*) (Figure 5, F and H), and collagen type X α 1 chain (*Col10a1*) (Figure 5, I and K), although biological variation between animals prevented statistical significance. Of note, we found that matrix GLA protein (*Mgp*), a negative regulator of endochondral and intramembranous ossification (18), tended to be elevated in untreated calluses of both mutant genotypes (Figure 5, J and L), and this was normalized by 24R,25$(OH)_2D_3$ treatment in *Cyp24a1*-null mice.

Discussion

Hydroxylation of 1,25$(OH)_2D_3$ on carbon 24 by CYP24A1 initiates the 24-oxidation pathway that leads to 1,25$(OH)_2D_3$ metabolite inactivation (3). 25$(OH)D_3$ can also serve as a substrate for the CYP24A1 enzyme, leading to the production of 24R,25$(OH)_2D_3$. A prevalent view has remained that, since it limits the synthesis of active 1,25$(OH)_2D_3$ from the 25$(OH)D_3$ precursor, the production of 24R,25$(OH)_2D_3$ by CYP24A1 enzymatic activity is a parallel inactivation route, and thus 24R,25$(OH)_2D_3$ should be considered a catabolite. However, an extensive literature demonstrates that *Cyp24a1* is expressed in growth plate chondrocytes and that cells from the growth plate respond to 24R,25$(OH)_2D_3$ in a cell maturation–dependent manner (19). Another aspect of bone biology in which investigators have sought to identify a role for

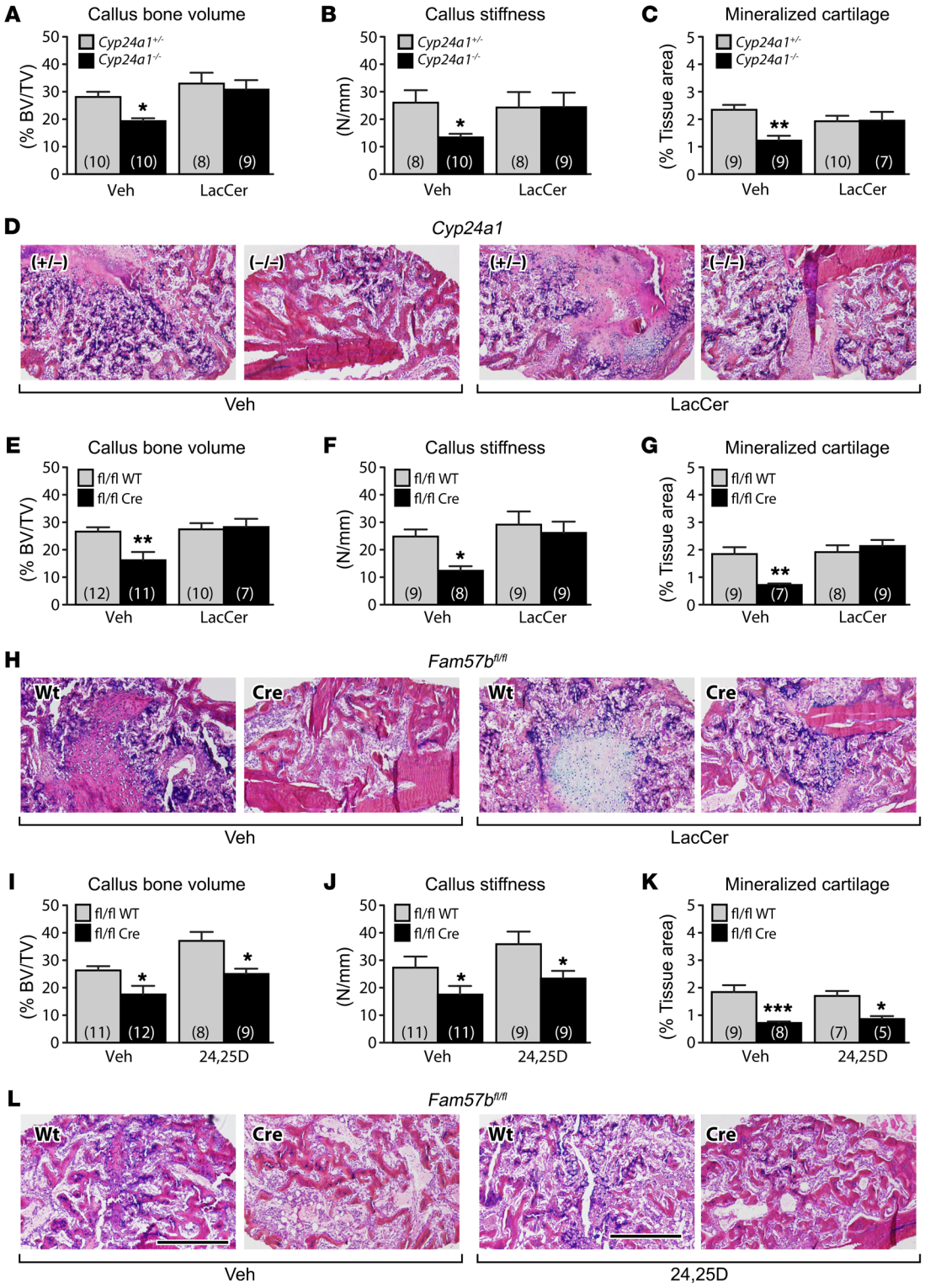

Figure 4. Rescue treatment with 24R,25(OH)$_2$D$_3$ or LacCer. Seventy-two hours after surgery, control (*Cyp24a1*$^{+/-}$ or fl/fl WT) and mutant (*Cyp24a1*$^{-/-}$ or fl/fl Cre) mice were subcutaneously injected once daily for fifteen days with vehicle, 6.7 μg/kg 24R,25(OH)$_2$D$_3$ (24,25D), or 50 μg/kg LacCer. Bone volume (**A**, **E**, and **I**) was calculated by micro-CT. Stiffness (**B**, **F**, and **J**) was calculated from 3PBTs. Mineralized cartilage area (**C**, **G**, and **K**) was calculated with ImageJ from histological sections stained with Alcian blue–H&E Y-Orange G trichrome (**D**, **H**, and **L**). *P < 0.05, **P < 0.01, and ***P < 0.001, by 2-way ANOVA followed by Bonferroni's post test. The number of animals per group is indicated in parentheses. Scale bars: 500 μm (**D**, **H**, and **L**).

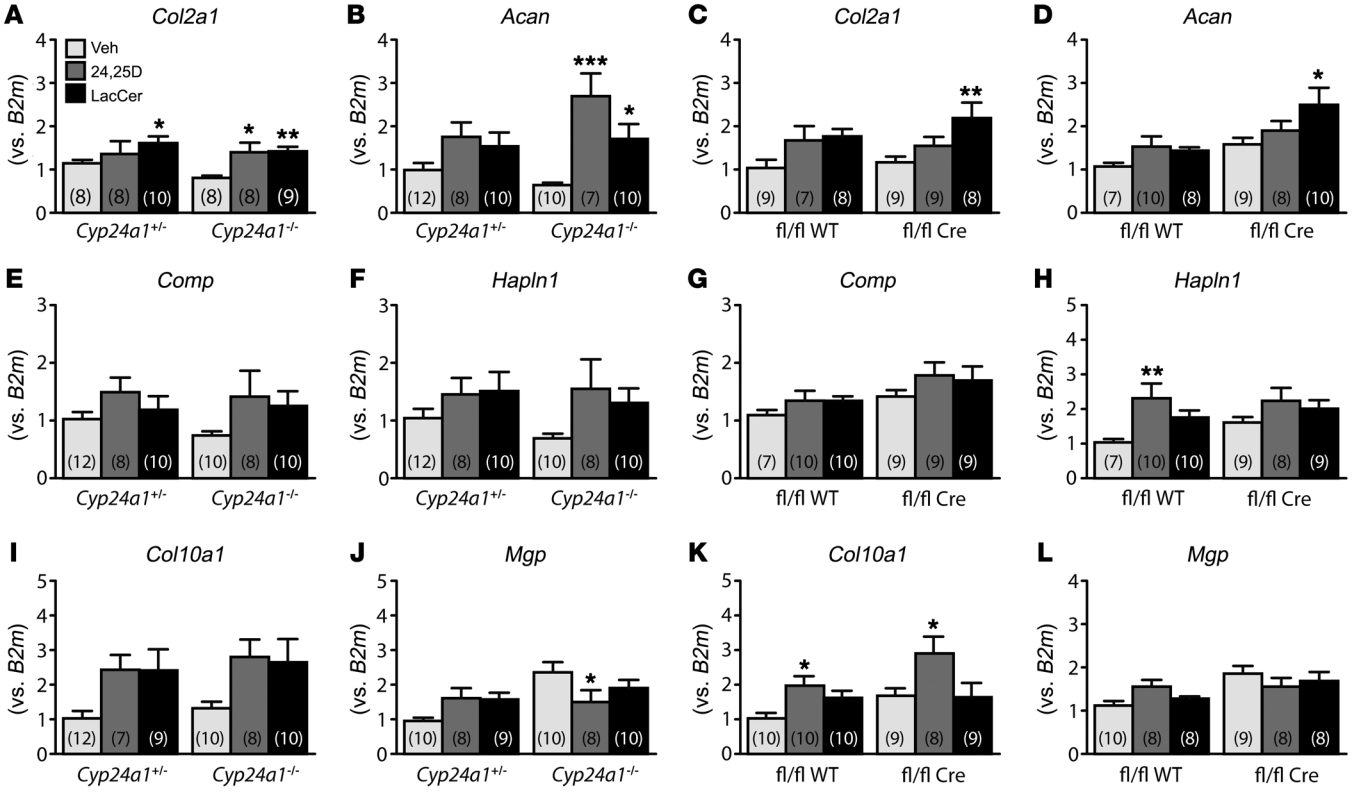

Figure 5. Expression monitoring of chondrogenic markers in repair callus. (**A**–**L**) RNA was isolated from day-18 repair callus. Relative expression levels of the genes indicated above each panel were determined by RT-qPCR and normalized to *B2m*. For each gene, expression in vehicle-treated controls was assigned a value of 1. *$P < 0.05$, **$P < 0.01$, and ***$P < 0.001$, by 2-way ANOVA followed by Bonferroni's post test. The number of animals per group is indicated in parentheses. 24,25D, daily subcutaneous injection of 6.7 μg/kg 24R,25$(OH)_2D_3$; LacCer, daily subcutaneous injection with 50 μg/kg C18-LacCer.

24R,25$(OH)_2D_3$ is fracture repair (6–8). Field observation data suggest that in the wild, long bone fractures in adults are rare and commonly fatal (20). Selection pressure to evolve an improved healing mechanism when the injury is uncommon and universally fatal is by definition slight (21). This may explain why multiple pathways act in parallel or redundantly to restore structure and function to broken bone tissue (22). The results reported herein characterize one such pathway.

We have used *Cyp24a1*-null mice (11) to study fracture repair in a 24R,25$(OH)_2D_3$-depleted mammalian system. These mice displayed suboptimal repair during the endochondral ossification phase. This interpretation is supported by the time point at which we measured a significant difference in callus volume (day 14 and day 18), which coincides with the time range of *Cyp24a1* expression in this tissue. In addition, previous results from our group show that distraction osteogenesis, whereby bone regeneration occurs predominantly through intramembranous bone formation (23), is not affected by *Cyp24a1* inactivation (24).

Comparing callus tissue gene expression between control and mutant animals allowed the cloning of *Fam57b* and the characterization of the chondrocyte-enriched FAM57B2 isoform. We present evidence of a genetic pathway involving 24R,25$(OH)_2D_3$-induced, FAM57B2-dependent LacCer production to optimize endochondral ossification during fracture repair. Our results argue against a VDR-mediated mechanism, since the circulating levels of 1,25$(OH)_2D_3$ were normal in the surviving *Cyp24a1*-null animals (Figure 1C and Supplemental Figure 1E) that had the impaired bone-healing phenotype. Moreover, treatment of marrow stromal cells with 1,25$(OH)_2D_3$ did not increase *Fam57b2* expression (data not shown), whereas elevated expression in the fracture callus was a criterion that allowed us to clone *Fam57b2*. Finally, neither 1,25$(OH)_2D_3$ nor 1,24,25$(OH)_3D_3$ induced FAM57B2-mediated LacCer production (Figure 3A). A VDR-independent mechanism for 24R,25$(OH)_2D_3$ in fracture healing is in agreement with the hypothesis originally proposed by Seo and Norman (8).

Human data on the role of 24R,25$(OH)_2D_3$ in bone healing are scarce. Available studies are limited to the measurement of circulating levels of vitamin D_3 metabolites at different intervals following fracture. The results are conflicting, with increases in serum 24R,25$(OH)_2D_3$ reported in young patients (25), while no changes were detected in older cohorts (26, 27). Though *CYP24A1* polymorphisms have been associated with human syndromes, the fracture risk does not seem to be increased, and it remains unknown whether any alteration in the fracture repair process occurs as a result of these polymorphisms. It would be informative to monitor bone healing following fracture as well as *FAM57B* isoform expression in patients with idiopathic infantile hypercalcemia (IIH) and Lightwood syndrome, which are caused by mutations in the *CYP24A1* gene (28–30).

The 24R,25$(OH)_2D_3$-induced production of LacCer by FAM57B2 shows features of allosteric enzymatic regulation, a well-established model for multimeric enzymes (31) that has also been demonstrated for monomeric enzymes (32). In allosteric enzyme regulation, the allosteric ligand binds in a specific, saturable manner at a site separate from the enzymatic active site, modifying the protein's conformation to modulate its activity (33). The allosteric modulator can regulate both the activity level and substrate specificity of the enzyme (31). The 24R,25$(OH)_2D_3$ effect was very specific and stereoselective, as neither the 1,25$(OH)_2D_3$ hormone, the 1,24,25$(OH)_3D_3$ metabolite, nor the non-natural 24S,25$(OH)_2D_3$ epimer (15, 16) could induce LacCer production. Our results also indicate a cooperative binding of 24R,25$(OH)_2D_3$ to FAM57B2, since a Hill coefficient of greater than 1 was calculated (13). However, structure-function analysis of the FAM57B2 protein remains to be performed to identify key residues for the enzymatic activity and to define the 24R,25$(OH)_2D_3$ binding pocket.

The 24R,25$(OH)_2D_3$ molecule is a circulating vitamin D_3 metabolite, and it remains unclear whether it needs to be synthesized at the fracture site to exert beneficial effects, or whether 24R,25$(OH)_2D_3$ from the circulation is sufficient. Given that chondrocytes are compartmentalized prior to vascularization of the repair callus, local synthesis of 24R,25$(OH)_2D_3$ may contribute significantly to the healing process. The question was not answered by our experiments, since the targeted mutation of the *Cyp24a1* allele that we generated led to global inactivation of the gene (11). Our data, however, indirectly indicate a contribution of local synthesis, since *Cyp24a1* expression was stimulated in callus tissue within the appropriate time range. The rescue treatment we used led to high circulating levels of 24R,25$(OH)_2D_3$ (Supplemental Figure 7B), which may have been necessary to allow access of the metabolite to the target cell in the hypovascularized callus. Considering that FAM57B2 is coexpressed in chondrocytes, we favor a model in which 24R,25$(OH)_2D_3$ acts via an intracrine (34) mechanism through endogenous synthesis in chondrocytes. Another potential source could be neighboring osteoblasts in paracrine signaling. Alternatively, injury macrophages, recently shown to be indispensable for efficient fracture repair (35), could represent a physiologically relevant source of the 24R,25$(OH)_2D_3$ metabolite. A floxed *Cyp24a1* allele and cell type–specific Cre drivers will be required to clarify this point. These experiments are in progress in our laboratory.

LacCer is the most important and abundant of the diosylceramides. It serves as the metabolic branch point for the formation of the different classes of complex glycosphingolipids in mammals (36, 37). In addition to its pivotal role in the biosynthesis of nearly all major glycosphingolipids, LacCer is also thought to regulate several aspects of cellular function (36). Specific signal transduction pathways involving LacCer have been characterized (36). These pathways have been shown to affect cell proliferation (38), adhesion (39, 40), apoptosis (41), and angiogenesis (42). Little is known about a specific role for LacCer in bone (43). We have initiated experiments to determine whether LacCer can modulate the proliferation, differentiation, or survival of chondrocytes.

Recent work from Boyan and colleagues (44) demonstrated that 24R,25$(OH)_2D_3$ prevents cartilage degradation during experimental osteoarthritis (OA), further supporting the chondrogenic properties of this metabolite. Since only the endochondral repair phase seems to be affected by *Cyp24a1* or *Fam57b* deletion, FAM57B2 might link vitamin D_3 metabolism to sphingolipid production to modulate *Col2a1* and *Acan* expression. Increasing evidence highlights the role of sphingolipids in cartilage homeostasis (45, 46). Indeed, sphingolipids have been shown to influence *Col2a1* expression (47) as well as chondrocyte apoptosis and matrix turnover (48).

The *Ugcg* gene encodes the enzyme that produces glucosylceramide (GluCer), which is the conventional precursor to LacCer. Chondrocyte-specific deletion of *Ugcg* showed that glycosphingolipids help to preserve cartilage integrity during experimental OA (49). The parallel between the OA models of Boyan (44) and Seito (49) indicates a correlation between 24R,25$(OH)_2D_3$ and glycosphingolipid production in cartilage homeostasis. Gangliosides, i.e., sialylated glycosphingolipids, are produced from LacCer (36) and are abundant in cartilage matrix (46). Gangliosides show a dual role in cartilage homeostasis, as their depletion can enhance cartilage repair by preventing chondrocyte hypertrophy (50) or accelerate its degradation during experimental OA (37).

Interestingly, a fracture repair study by Momma and colleagues (51) performed in Col2-Cre *Ugcg*-floxed mice showed a more severe phenotype than that described here. We hypothesize that *Cyp24a1*-null and Col2-Cre *Fam57b*$^{fl/fl}$ mice only partially phenocopy the Col2-Cre *Ugcg*$^{fl/fl}$ mouse, because GluCer synthesis remains unaffected. Moreover, since global glycosphingolipid metabolism remains intact in Col2-Cre *Fam57b*-floxed mice, our results suggest that LacCer production through the 24R,25$(OH)_2D_3$/FAM57B2 pathway might represent a local mechanism solicited in stress-related contexts such as healing and OA. These 2 pathways are probably redundant mechanisms that act to maximize the outcome of bone healing. LacCer synthesis classically occurs through galactosyl transfer onto a GluCer substrate (36). However, FAM57B2 has very little sequence homology with characterized LacCer synthases and further requires sphingosine (and not GluCer) as a substrate to produce LacCer following 24R,25$(OH)_2D_3$ binding. We surmise that GluCer treatment could ameliorate fracture repair but that this would occur through FAM57B2-independent mechanisms.

Few data exist concerning the function of FAM57B2. In adipocytes, *Fam57b* was identified as a transcriptional target of PPARγ, a member of the nuclear receptor family of transcription factors. The authors have shown that FAM57B2 inhibits adipogenesis (14). This is particularly interesting in the context of recent results showing that high callus adiposity is associated with delayed fracture healing and weakened biomechanical properties (52). Thus, inhibition of adipogenesis by FAM57B2 could play a beneficial role during fracture repair. The high constitutive expression of *Fam57b2* in skin (Supplemental Figure 4B) hints at the possibility that FAM57B2 might also play a role in keratinocyte differentiation or skin wound repair. In humans, the *FAM57B* gene was found to be expressed at higher levels in individuals who heal normally when compared with those suffering non-union fractures (Gene Expression Omnibus [GEO] GDS369, accessible at www.ncbi.nlm.nih.gov/sites/GDSbrowser?acc=GDS369), indicating a role in fracture repair. Though both isoforms 1 and 2 are associated with ceramide production in vitro (14), allosteric modulation toward LacCer synthesis by 24R,25$(OH)_2D_3$ appears to be specific to isoform 2. An

in-depth understanding of FAM57B2 structure and function could yield a novel therapeutic target for fracture repair as well as OA. Alternatively, treatment with 24R,25$(OH)_2D_3$ [or 24R,25$(OH)_2D_3$ analogs] or with LacCer could represent a novel approach for the therapeutic management of fractures.

Methods

Animals and feeding. Mice were housed under a 12-hour light/12-hour dark cycle and maintained at 25°C with free access to food and water. The *Cyp24a1*-null mouse strain has been described previously (11) and was maintained on a mixed genetic background (129Sv/C57BL6) for 69 generations. To maximize the number of test animals available for the study, breeding pairs consisted of homozygous mutant males (*Cyp24a1*$^{-/-}$) mated with heterozygous females (*Cyp24a1*$^{+/-}$). The resulting progeny consisted of control heterozygous animals and mutant homozygous *Cyp24a1*-null mice; the test cohorts were composed of female littermates. The *Cyp24a1*$^{+/-}$ mice have a WT phenotype and were adequate controls, as shown by comparing serum biochemistry values (Supplemental Figure 1), metabolism (Supplemental Figure 2), and body composition (Supplemental Table 1) between *Cyp24a1*$^{+/+}$, *Cyp24a1*$^{+/-}$, and *Cyp24a1*$^{-/-}$ littermates.

The *Fam57b*-targeted allele is based on the International Knockout Mouse Consortium's knockout first reporter–tagged insertion promotor–driven cassette (53) and targets exon 6 within *Fam57b*, producing a null allele. Embryonic stem (ES) cells carrying the floxed allele were purchased from the European Conditional Mouse Mutagenesis Program (EUCOMM) (Neuherberg, Germany) and injected into C57BL6 blastocysts at the core facility of the Centre Hospitalier de l'Université de Montréal. Chimeric males were bred with C57BL6 females, and germline transmission was confirmed by PCR analysis from tail-snip DNA (54). Heterozygotes for the floxed allele were interbred to produce animals of all 3 possible genotypes (+/+, +/fl, and fl/fl). Subsequent breeding involved the Col2-Cre–transgenic mouse strain (17): Col2-Cre mice were bred with *Fam57b*$^{fl/fl}$ mice to obtain mice carrying the Cre transgene and 1 floxed allele (genotype: Col2-Cre *Fam57b*$^{+/fl}$). These were mated with homozygotic floxed mice to obtain the test genotype:Col2- Cre *Fam57b*$^{fl/fl}$ and littermate controls; the phenotype of the male and female experimental cohorts from the 15th generation was examined separately. The predominant FAM57B isoform in chondrocytes is the 24R,25$(OH)_2D_3$-binding FAM57B2 protein. Expression of *Fam57b1*, *-2*, and *-3* in other tissues remained unaffected (Supplemental Figure 4 and data not shown).

Serum biochemistry. Total serum calcium and serum phosphate levels were measured using an automated analyzer. Serum levels of vitamin D metabolites were assayed by liquid chromatography–tandem mass spectrometry (LC-MS/MS) following DMEQ-TAD derivatization as described previously (55). Briefly, serum aliquots and calibrators were diluted 1:3 with water and spiked with internal standards. Proteins were precipitated by sequentially adding 0.1 M HCl, 0.2 M zinc sulfate, and 40 μl methanol, with vortexing after the addition of each component. Tubes were centrifuged for 10 minutes at 12,000 *g*, and supernatants were transferred to borosilicate glass tubes. Organic extraction was carried out by adding equal volumes of hexane and methyl tertiary butyl ether with vortexing after the addition of each component. The upper organic phase was transferred into LC-MS/MS sample vials and evaporated under nitrogen flow. Dried residues were derivatized by addition of 0.1 mg/ml DMEQ-TAD dissolved in ethyl acetate for 30 minutes at room temperature in the dark and then a second time for 60 minutes. The reaction was stopped by addition of ethanol, and the samples were dried and redissolved in 60:40 methanol/water running buffer. LC-MS/MS analysis was performed using an Acquity UPLC connected in-line with a Xevo TQ-S mass spectrometer in electrospray-positive mode (Waters Corporation). Through a Queen's University and Waters Corporation agreement, Waters provided the LC-MS/MS instrument used in this study. Chromatographic separations were achieved using a BEH-phenyl ultra-performance LC (UPLC) column (1.7 μm, 2.1 × 50 mm) (Waters) and a methanol-water–based gradient solvent system.

Micro-CT. Calluses and contralateral tibiae were harvested in PBS, scanned with a model 1272 SkyScan micro-CT system (Bruker) at 65 kV, 142 μAmp, 5-μm resolution, and a 0.5° rotation using a 0.5-mm aluminum filter, and frozen at –20°C until 3-point bending tests (3PBTs). Raw data sets were reconstructed with InstaRecon software (Bruker) and analyzed with CTAn software (Bruker). Volumes of interest consisted of 400 slices (2-mm-thick) above and below the osteotomy site and used to obtain the mineralized callus volume (percentage of bone volume to tissue volume [BV/TV]). Tissue volume was set as a 20-mm^3 rectangular prism. Contralateral tibiae were analyzed to ensure minimal impact of the genotype and treatment under basal conditions.

Intramedullary rodded tibial osteotomy. Twelve-week-old *Cyp24a1*-null, Col2-Cre *Fam57b*$^{fl/fl}$, and control littermate mice were preoperatively injected with buprenorphine (0.1 mg/kg; Chiron Compounding Pharmacy) and underwent isoflurane general anesthesia. Skin was incised above the left knee, and the patellar ligament was detached from the lateral tissue on both sides. The tibial plateau was perforated under the ligament with a 26-gauge needle (Terumo), and a 25-gauge internal spinal wire guide (BD) was inserted down the medullary canal. The needle was pulled out, and the wire guide was bent 90° and cut at the tibial plateau, and then secured under the ligament with stitching (5-0; Ethicon). The tibial mid-shaft was exposed, and osteotomy was performed 2–3 mm above the tibiofibular junction using scissors. A drop of a 1:1 mix of 1% lidocaine (Zoetis) and 1% bupivicaine (Hospira) was topically applied, and the skin was sutured. Mice were injected with 0.05 mg/kg carprofen (Zoetis) at the time of surgery and postoperatively if they exhibited signs of pain during the next 48-hour period. Animals were sacrificed at intervals (10, 14, 18, 21, or 28 days) after surgery (indicated in the figures). For euthanasia, the mice were given a lethal injection of a ketamine (Vetoquinol), xylazine (Bayer), and acepromazine (Boehringer Ingelheim) cocktail before exsanguination, followed by cervical dislocation prior to dissection. Calluses and contralateral tibiae were harvested for analysis.

Osteotomy with external fixator. The surgical procedure for installation of the miniature distraction osteogenesis apparatus designed by Tay et al. (56) has been described previously (57). The apparatus was used without distraction as an external static fixator for osteotomy healing on 12-week-old mice.

Rescue treatment with 24R,25$(OH)_2D_3$, 1,25$(OH)_2D_3$ or LacCer. For rescue experiments, mice were subcutaneously injected for 15 days, starting 72 hours after surgery, with either 24R,25$(OH)_2D_3$ (6.7 μg/kg daily in 50 μl propylene glycol with trace ethanol for vitamin D metabolite solubility); 1,25$(OH)_2D_3$ (67 ng/kg); or propylene glycol (with trace ethanol) vehicle. The difference in the rescue doses of the 2 metabolites is based on the fact that systemic levels of 1,25$(OH)_2D_3$ are 10- to 100-fold lower than circulating levels of 24R,25$(OH)_2D_3$ under normal physiological conditions (58)

and to avoid hypervitaminosis and hypercalcemia in $1,25(OH)_2D_3$-treated *Cyp24a1*-null mice (11). The levels of $24R,25(OH)_2D_3$ were measured by LC-MS/MS following rescue treatment and found to be 4-fold higher in the treated *Cyp24a1*$^{-/-}$ mice as compared with the treated controls (197 ± 31 ng/ml vs. 827 ± 147 ng/ml; $P < 0.001$, control vs. mutant; $n = 6$, respectively) (Supplemental Figure 7B). This treatment also significantly decreased $1,25(OH)_2D_3$ and increased $1,24,25(OH)_3D_3$ in both genotypes (Supplemental Figure 7, C and D).

Rescue with LacCer used C18-LacCer at 50 μg/kg daily in 50 μl propylene glycol with trace DMSO for solubility or the propylene glycol with trace DMSO vehicle until sacrifice. LacCer injections had no detectable impact on any of the circulating vitamin D_3 metabolites levels measured (Supplemental Figure 7).

Gene expression monitoring. Calluses were harvested at specified time points (see figure legends), collected in RNAlater (Invitrogen, Thermo Fisher Scientific) and used for total RNA extraction in QIAzol (QIAGEN). Resuspended RNA was cleansed using the QIAGEN RNA Protect Kit, and 260:280 and 260:230 ratios were evaluated with NanoDrop (Thermo Fisher Scientific). RNA samples with a 260:280 ratio above 1.9 and 260:230 ratios above 2 were reverse transcribed using the High-Capacity cDNA Reverse Transcription Kit (Applied Biosystems), and gene expression was assessed in a QuantStudio 7 Flex apparatus (Applied Biosystems) using Taqman-specific probes for β-microglobulin (*B2m*), *Acan*, *Col2a1*, *Col10a1*, *Mgp*, *Comp*, and *Hapnl1*, as well as *Cyp24a1*, *Fam57b1*, and *Fam57b2* (Applied Biosystems).

3PBTs. For the 3PBTs, contralateral and callus tibiae were thawed overnight at room temperature and tested for mechanical properties using an Instron model 5943 single-column table frame machine. A load-sensing cell was applied on the widest part of the callus, or 2 to 3 mm above the tibiofibular junction in the case of intact tibiae, which were held by holders set 6 mm apart. The raw output used for comparison was stiffness (N/mm).

Gene expression monitoring using microarrays. RNA samples from day 14 calluses from control and *Cyp24a1*-null mice were sent to the Genome Quebec and McGill University Innovation Centre (Montreal, Quebec, Canada) for microarray analysis. Briefly, RNA quality was assessed as described above, and first- and second-strand cDNAs were synthesized, followed by complementary RNA (cRNA) amplification and purification. Second-cycle single-stranded cDNA was synthesized and purified and then fragmented and biotinylated. Labeled cDNA was then hybridized on a GeneChip MOE430 2.0 (Affymetrix, Applied Biosystems). The resulting data allowed the identification of 4 genes using the following criteria: (a) selective overexpression in *Cyp24a1*-null tissue; (b) sequences coding for membrane-associated proteins; and/or (c) sequences coding for proteins of unknown function (Supplemental Table 2; the complete data set has been deposited in the Gene Expression Omnibus repository under the accession number GEO GSE112449).

Cloning and expression of candidate genes. Full-length cDNAs corresponding to the genes identified by microarrays (GenBank accession numbers AK005271, AK005126, AK003840, and AK009853) were obtained from the RIKEN Cell Bank and cloned inside a modified pBluescript SK plasmid (Stratagene) using competent bacteria, and then subcloned into the pcDNA3.1 (Invitrogen, Thermo Fisher Scientific) mammalian expression vector to generate stable COS7 cells (American Type Culture Collection [ATCC]) through G418 selection. Transfected cells were expanded as needed and maintained in DMEM supplemented with 10% FBS.

Binding assays. Membrane fractions were prepared as described by Patino and Thomas (59). Briefly, transfected COS7 cells were harvested in ice-cold HAED buffer (25 mM HEPES, pH 7.6, 10 mM NaCl, 1 mM dithiothreitol, 1 mM EDTA) containing protease inhibitors, sonicated with 3 short bursts, and sequentially centrifuged for 7 minutes at 1,000 *g* and then for 20 minutes at 20,000 *g*. The resulting pellets were solubilized in HAED buffer to 1 mg/ml and kept on ice until use in the binding assays. Membrane fractions (200–400 μg in 250 μl) were incubated in a range of $[^3H]$-$24R,25(OH)_2D_3$ (specific activity: 174 Ci/mmol; New England Nuclear Life Sciences Products) concentrations (0.025–5 nM) dissolved in 250 μl HAED buffer with (nonspecific) or without (total) a 200-fold excess of nonradioactive $24R,25(OH)_2D_3$ for 30 minutes at 4°C. Bound steroid was separated from free steroid by filtration (Whatman GF/B; pore size 1 μm). Filters were washed and radioactivity was counted in a liquid scintillation counter. The K_D, Hill coefficient (H), and binding capacity (Bmax) were estimated from specific binding saturation analyses. Competitive binding assays were conducted over the concentration range of 10^{-10} to 10^{-5} M competitor incubated with 5 nM $[^3H]$-$24R,25(OH)_2D_3$ for 30 minutes. Competition was expressed as a percentage of the maximal specific binding and used to estimate the K_i (57).

Overexpression of FAM57B2. The coding sequence for murine *Fam57b2* was inserted into the pcDNA3.1 plasmid (Invitrogen, Thermo Fisher Scientific) and transfected into HEK293 cells (ATCC) using lipofectamine, in parallel with an empty construct, using 5 μg DNA per 100-mm dish of 50% confluent cells in 5 ml FBS-free DMEM. Cells were incubated for 2 hours at 37°C before adding 5 ml of 20% FBS DMEM and then incubated at 37°C in vitamin D_3–depleted serum for 72 more hours. The transiently transfected cells were then used for analysis.

LacCer production assay. Confluent cells were rinsed twice with cold PBS and then harvested in 300 μl ice-cold assay buffer (250 mM sucrose, 20 mM HEPES, pH 7.6, 36 mM KCl, 2 mM $MgCl_2$) supplemented with 1× protease inhibitor cocktail (MilliporeSigma) and 1 mM PMSF, followed by sonication for 1 minute at 30% intensity (10 s on/off). The enzymatic assay (modified from ref. 14) was performed with 100 μg cell lysate diluted in 25 μl assay buffer and preincubated with 25 μl 4× mixtures (4 μM) of $25(OH)D_3$ (MilliporeSigma); $1,24,25(OH)_3D_3$ (Carbosynth); $24R,25(OH)_2D_3$ (MedChem Express); $1,25(OH)_2D_3$ (Toronto Research Chemicals); $24S,25(OH)_2D_3$ (provided by A. Norman, University of California, Riverside, California, USA); or vehicle control (95% ethyl alcohol [ETOH]) on ice for 30 minutes. The reaction was completed to 100 μl by adding 50 μl of a 2× assay mix containing 30 μM D-erythro-sphingosine (Avanti Polar Lipids), 40 μM fatty acid-free BSA (MilliporeSigma), 100 μM of 18:0 coenzyme A (Avanti Polar Lipids), and 1× antiprotease mix. The reactions were launched for 30 minutes at 37°C, stopped by adding 0.5 ml 100% methanol, and then the samples were stored at –20°C until analysis.

Lipid extraction and thin-layer chromatography. Lipids were extracted by Folch's partition method (60). Briefly, samples were mixed with chloroform/methanol/water in a 2:1:0.8 ratio, with vortexing between the addition of each component. Samples were vortexed at maximum speed for 10 seconds, and phase separation was completed with centrifugation (2,000 *g*, 1 min). Aqueous phases were discarded, and organic phases were evaporated under N2(g). The remaining film was dissolved in 30 μl of methanol/chloroform (1:1) and loaded onto thin-layer chromatography (TLC) plates that were developed using (50:42:10) chloroform/methanol/0.2% $CaCl_2$(aq) as a mobile phase. Lipids were

revealed with 10% copper sulfate in 8% phosphoric acid, followed by charring in a toaster oven set at 200°F for 5 to 10 minutes. Sphingosine (Sp), LacCer, phosphatidylcholine (PC), and phosphatidylethanolamine (PE) were loaded as standards (Avanti Polar Lipids).

Primary chondrocyte isolation. The procedure was modified from that of Mackay et al. (61). Briefly, femoral and tibial articular cartilage from 8-week-old *Cyp24a1*-null mice and age-matched littermates was dissected and cleansed of soft tissue under sterile conditions, followed by a 1-hour predigestion in 1 mg/ml collagenase I from *C. histolyticum* (MilliporeSigma) at 37°C to eliminate the remaining soft tissue. Cartilage was then cut into small pieces and sequentially digested in 200 μg/ml collagenase I in DMEM 3 times for 24 hours with vigorous agitation at 37°C. Between each digestion, supernatants were harvested and strained (80-μm) before plating in DMEM supplemented with 10% FBS. Adherent cells were thoroughly washed with PBS and expanded.

Treatment of chondrocytes with LacCer or 24R,25(OH)$_2$D$_3$. Chondrocytes were plated in 12-well plates, and at confluence, the medium was changed for DMEM, without FBS, supplemented with 1 μM LacCer, 100 nM 24R,25(OH)$_2$D$_3$, or vehicle for 24 hours. The cells were rinsed twice with PBS, and RNA was extracted using QIAzol reagent according to the manufacturer's protocol. RNA was reverse transcribed, and *Fam57b2* expression was monitored using specific probes (Applied Biosystems) and normalized to *B2m*.

Histology. Bones were fixed in 70% ethanol with 1% glycerol and kept at –20°C until processing. Bones were dehydrated at 4°C and infiltrated with low-temperature polymerizing methylmethacrylate (MMA) solutions 1, 2, and 3 as described by Erben (62). Bones were embedded in MMA solution 3 supplemented with 0.4% 4-*N*,*N*,*N*,*N*-trimethylaniline (MilliporeSigma) and left to polymerize at –20°C for 3 days under N_2(g) atmosphere. Blocks were sectioned at 5-μm thickness using a rotary microtome equipped with a tungsten blade (Leica), stretched onto poly-L-lysine–coated superfrost slides, stacked with plastic clamps, and left to dry overnight at room temperature. For staining, sections were deplastified in xylene (1 h), ethylene glycol monoethyl ether acetate (EGMA) (1 h), and acetone (10 min) and then rehydrated with water and stained with Alcian blue H&E Y-orange G trichrome. Images were taken using a Leica DMR microscope (Leica Microsystems) connected to a digital DP70 camera (Olympus), and analyses were performed using ImageJ software (NIH).

Statistics. Binding and statistical analyses were performed with GraphPad Prism 5 (GraphPad Software). One-site specific binding with a Hill slope equation was used in saturation analyses to estimate K_D, H, and Bmax values; a one-site fit K_i equation was used in competition analyses to estimate K_i values. The ROUT test in GraphPad Prism was applied to eliminate outliers from the nonlinear regression using a Q value of 0.01. Statistical analyses were performed using a 2-tailed t test or a 1-way or 2-way ANOVA, followed by Dunnett's or Bonferroni's post hoc test. Outliers were identified using the Grubbs test (extreme studentized deviate). The statistical significance threshold was set at a P value of less than 0.05. All data are presented as the mean ± SEM.

Study approval. The animal use protocol (AUP 4138) and all standard operating procedures were approved by the IACUC of Shriners Hospitals for Children – Canada, as part of the McGill University animal ethics and care program, and followed the guidelines of the Canadian Council on Animal Care.

Author contributions

CM, RPN, AH, BH, MK, and AA generated data. CM, GJ, and RStA participated in data analysis and interpretation. OA provided materials and technical support. RStA obtained the funding. CM and RStA participated in the conception and design of the study and wrote the manuscript.

Acknowledgments

This work was supported in part by grant 85600 from Shriners Hospitals for Children (to RStA) and by NIH grant R01AR070544 (to RStA). CM is a postdoctoral fellow of the Fonds de Recherche Québec – Santé. We thank Mia Esser and Louise Marineau (Shriners Hospitals for Children – Canada) for expert animal care, as well as Claude Gauthier (Shriners Hospitals for Children – Canada) and Mary Traynor (Queen's University) for technical assistance.

Address correspondence to: René St-Arnaud, Research Centre, Shriners Hospitals for Children – Canada 1003 Decarie Boulevard, Montreal, Quebec, Canada H4A 0A9. Phone: 514.282.7155; Email: rst-arnaud@shriners.mcgill.ca.

1. Horst RL, Reinhardt TA, Reddy GS. Vitamin D metabolism. In: Feldman D, Pike JW, Glorieux FH, eds. *Vitamin D*. 2nd ed. San Diego: Elsevier Academic Press; 2005:15–36.
2. Sutton AL, MacDonald PN. Vitamin D: more than a "bone-a-fide" hormone. *Mol Endocrinol*. 2003;17(5):777–791.
3. Makin G, Lohnes D, Byford V, Ray R, Jones G. Target cell metabolism of 1,25-dihydroxyvitamin D3 to calcitroic acid. Evidence for a pathway in kidney and bone involving 24-oxidation. *Biochem J*. 1989;262(1):173–180.
4. Jones G, Prosser DE, Kaufmann M. 25-Hydroxyvitamin D-24-hydroxylase (CYP24A1): its important role in the degradation of vitamin D. *Arch Biochem Biophys*. 2012;523(1):9–18.
5. St-Arnaud R. CYP24A1: structure, function, and physiological role. In: Feldman D, Pike JW, Adams JS eds. *Vitamin D*. 2nd ed. San Diego: Academic Press; 2011:43–56.
6. Seo EG, Einhorn TA, Norman AW. 24R,25-dihydroxyvitamin D3: an essential vitamin D3 metabolite for both normal bone integrity and healing of tibial fracture in chicks. *Endocrinology*. 1997;138(9):3864–3872.
7. Seo EG, Kato A, Norman AW. Evidence for a 24R,25(OH)2-vitamin D3 receptor/binding protein in a membrane fraction isolated from a chick tibial fracture-healing callus. *Biochem Biophys Res Commun*. 1996;225(1):203–208.
8. Seo EG, Norman AW. Three-fold induction of renal 25-hydroxyvitamin D3-24-hydroxylase activity and increased serum 24,25-dihydroxyvitamin D3 levels are correlated with the healing process after chick tibial fracture. *J Bone Miner Res*. 1997;12(4):598–606.
9. Marsell R, Einhorn TA. The biology of fracture healing. *Injury*. 2011;42(6):551–555.
10. Kato A, Seo EG, Einhorn TA, Bishop JE, Norman AW. Studies on 24R,25-dihydroxyvitamin D3: evidence for a nonnuclear membrane receptor in the chick tibial fracture-healing callus. *Bone*. 1998;23(2):141–146.
11. St-Arnaud R, et al. Deficient mineralization of intramembranous bone in vitamin D-24-hydroxylase-ablated mice is due to elevated 1,25-dihydroxyvitamin D and not to the absence of 24,25-dihydroxyvitamin D. *Endocrinology*. 2000;141(7):2658–2666.
12. Fukaya N, Ito M, Iwata H, Yamagata T. Characterization of the glycosphingolipids of pig cortical bone and cartilage. *Biochim Biophys Acta*. 1989;1004(1):108–116.
13. Prinz H. Hill coefficients, dose-response curves and allosteric mechanisms. *J Chem Biol*. 2010;3(1):37–44.
14. Yamashita-Sugahara Y, et al. Fam57b (family with

sequence similarity 57, member B), a novel peroxisome proliferator-activated receptor γ target gene that regulates adipogenesis through ceramide synthesis. *J Biol Chem*. 2013;288(7):4522–4537.
15. Tanaka Y, DeLuca HF, Ikekawa N, Morisaki M, Koizumi N. Determination of stereochemical configuration of the 24-hydroxyl group of 24,25-dihydroxyvitamin D3 and its biological importance. *Arch Biochem Biophys*. 1975;170(2):620–626.
16. Tanaka Y, Frank H, DeLuca HF, Koizumi N, Ikekawa N. Importance of the stereochemical position of the 24-hydroxyl to biological activity of 24-hydroxyvitamin D3. *Biochemistry*. 1975;14(15):3293–3296.
17. Terpstra L, et al. Reduced chondrocyte proliferation and chondrodysplasia in mice lacking the integrin-linked kinase in chondrocytes. *J Cell Biol*. 2003;162(1):139–148.
18. Yagami K, et al. Matrix GLA protein is a developmental regulator of chondrocyte mineralization and, when constitutively expressed, blocks endochondral and intramembranous ossification in the limb. *J Cell Biol*. 1999;147(5):1097–1108.
19. Boyan BD, Schwartz Z. Cartilage and vitamin D: genomic and nongenomic regulation by $1,25(OH)_2D_3$ and $24,25(OH)_2D_3$. In: Feldman D, Pike JW, Glorieux FH eds. *Vitamin D*. 2nd ed. San Diego: Elsevier Academic Press; 2005:575–597.
20. Bulstrode C, King J, Roper B. What happens to wild animals with broken bones? *Lancet*. 1986;1(8471):29–31.
21. Aspenberg P. Drugs and fracture repair. *Acta Orthop*. 2005;76(6):741–748.
22. Einhorn TA, Gerstenfeld LC. Fracture healing: mechanisms and interventions. *Nat Rev Rheumatol*. 2015;11(1):45–54.
23. Aronson J. Experimental and clinical experience with distraction osteogenesis. *Cleft Palate Craniofac J*. 1994;31(6):473–481; discussion 481.
24. Husseini A, St-Arnaud R. CYP24A1-deficiency does not affect bone regeneration in distraction osteogenesis. *J Steroid Biochem Mol Biol*. 2017;173:168–172.
25. Meller Y, et al. Parathyroid hormone, calcitonin, and vitamin D metabolites during normal fracture healing in humans. A preliminary report. *Clin Orthop Relat Res*. 1984;(183):238–245.
26. Briggs AD, et al. Longitudinal study of vitamin D metabolites after long bone fracture. *J Bone Miner Res*. 2013;28(6):1301–1307.
27. Meller Y, et al. Parathormone, calcitonin, and vitamin D metabolites during normal fracture healing in geriatric patients. *Clin Orthop Relat Res*. 1985;(199):272–279.
28. Castanet M, Mallet E, Kottler ML. Lightwood syndrome revisited with a novel mutation in CYP24 and vitamin D supplement recommendations. *J Pediatr*. 2013;163(4):1208–1210.
29. Marks BE, Doyle DA. Idiopathic infantile hypercalcemia: case report and review of the literature. *J Pediatr Endocrinol Metab*. 2016;29(2):127–132.
30. Schlingmann KP, et al. Mutations in CYP24A1 and idiopathic infantile hypercalcemia. *N Engl J Med*. 2011;365(5):410–421.
31. Traut TW. *Allosteric Regulatory Enzymes*. New York: Springer US; 2008.
32. Kamata K, Mitsuya M, Nishimura T, Eiki J, Nagata Y. Structural basis for allosteric regulation of the monomeric allosteric enzyme human glucokinase. *Structure*. 2004;12(3):429–438.
33. Brown NC, Reichard P. Role of effector binding in allosteric control of ribonucleoside diphosphate reductase. *J Mol Biol*. 1969;46(1):39–55.
34. Labrie F, et al. Intracrinology: role of the family of 17 beta-hydroxysteroid dehydrogenases in human physiology and disease. *J Mol Endocrinol*. 2000;25(1):1–16.
35. Raggatt LJ, et al. Fracture healing via periosteal callus formation requires macrophages for both initiation and progression of early endochondral ossification. *Am J Pathol*. 2014;184(12):3192–3204.
36. Chatterjee S, Pandey A. The Yin and Yang of lactosylceramide metabolism: implications in cell function. *Biochim Biophys Acta*. 2008;1780(3):370–382.
37. Sasazawa F, et al. Depletion of gangliosides enhances cartilage degradation in mice. *Osteoarthr Cartil*. 2014;22(2):313–322.
38. Bhunia AK, Han H, Snowden A, Chatterjee S. Lactosylceramide stimulates Ras-GTP loading, kinases (MEK, Raf), p44 mitogen-activated protein kinase, and c-fos expression in human aortic smooth muscle cells. *J Biol Chem*. 1996;271(18):10660–10666.
39. Bhunia AK, Arai T, Bulkley G, Chatterjee S. Lactosylceramide mediates tumor necrosis factor-alpha-induced intercellular adhesion molecule-1 (ICAM-1) expression and the adhesion of neutrophil in human umbilical vein endothelial cells. *J Biol Chem*. 1998;273(51):34349–34357.
40. Gong N, Wei H, Chowdhury SH, Chatterjee S. Lactosylceramide recruits PKCalpha/epsilon and phospholipase A2 to stimulate PECAM-1 expression in human monocytes and adhesion to endothelial cells. *Proc Natl Acad Sci U S A*. 2004;101(17):6490–6495.
41. Martin SF, Williams N, Chatterjee S. Lactosylceramide is required in apoptosis induced by N-Smase. *Glycoconj J*. 2006;23(3-4):147–157.
42. Kolmakova A, Rajesh M, Zang D, Pili R, Chatterjee S. VEGF recruits lactosylceramide to induce endothelial cell adhesion molecule expression and angiogenesis in vitro and in vivo. *Glycoconj J*. 2009;26(5):547–558.
43. Iwamoto T, et al. Lactosylceramide is essential for the osteoclastogenesis mediated by macrophage-colony-stimulating factor and receptor activator of nuclear factor-kappa B ligand. *J Biol Chem*. 2001;276(49):46031–46038.
44. Boyan BD, et al. 24R,25-Dihydroxyvitamin D3 protects against articular cartilage damage following anterior cruciate ligament transection in male rats. *PLoS ONE*. 2016;11(8):e0161782.
45. Khavandgar Z, Murshed M. Sphingolipid metabolism and its role in the skeletal tissues. *Cell Mol Life Sci*. 2015;72(5):959–969.
46. Rocha B, et al. Characterization of lipidic markers of chondrogenic differentiation using mass spectrometry imaging. *Proteomics*. 2015;15(4):702–713.
47. Gilbert SJ, Blain EJ, Duance VC, Mason DJ. Sphingomyelinase decreases type II collagen expression in bovine articular cartilage chondrocytes via the ERK signaling pathway. *Arthritis Rheum*. 2008;58(1):209–220.
48. Sabatini M, et al. Effects of ceramide on apoptosis, proteoglycan degradation, and matrix metalloproteinase expression in rabbit articular cartilage. *Biochem Biophys Res Commun*. 2000;267(1):438–444.
49. Seito N, et al. Interruption of glycosphingolipid synthesis enhances osteoarthritis development in mice. *Arthritis Rheum*. 2012;64(8):2579–2588.
50. Matsuoka M, et al. Depletion of gangliosides enhances articular cartilage repair in mice. *Sci Rep*. 2017;7:43729.
51. Momma D, Takahata M, Kameda Y, Shimizu T, and Iwasaki N. Interruption of glycosphingolipid synthesis decelerates endochondral ossification in fracture healing. Presented at: ORS 2015; Las Vegas, Nevada, USA; 2015. http://www.ors.org/Transactions/61/1497.pdf. Accessed July 6, 2018.
52. Brown ML, et al. Delayed fracture healing and increased callus adiposity in a C57BL/6J murine model of obesity-associated type 2 diabetes mellitus. *PLoS One*. 2014;9(6):e99656.
53. Testa G, et al. A reliable lacZ expression reporter cassette for multipurpose, knockout-first alleles. *Genesis*. 2004;38(3):151–158.
54. Laird PW, Zijderveld A, Linders K, Rudnicki MA, Jaenisch R, Berns A. Simplified mammalian DNA isolation procedure. *Nucleic Acids Res*. 1991;19(15):4293.
55. Kaufmann M, et al. Clinical utility of simultaneous quantitation of 25-hydroxyvitamin D and 24,25-dihydroxyvitamin D by LC-MS/MS involving derivatization with DMEQ-TAD. *J Clin Endocrinol Metab*. 2014;99(7):2567–2574.
56. Tay BK, Le AX, Gould SE, Helms JA. Histochemical and molecular analyses of distraction osteogenesis in a mouse model. *J Orthop Res*. 1998;16(5):636–642.
57. Haque T, et al. Characterizing the BMP pathway in a wild type mouse model of distraction osteogenesis. *Bone*. 2008;42(6):1144–1153.
58. Hollis BW. Detection of vitamin D and its major metabolites. In: Feldman D, Pike JW, Adams JS, eds. *Vitamin D*. San Diego: Academic Press; 2011:823–844.
59. Patiño R, Thomas P. Characterization of membrane receptor activity for 17 alpha, 20 beta, 21-trihydroxy-4-pregnen-3-one in ovaries of spotted seatrout (Cynoscion nebulosus). *Gen Comp Endocrinol*. 1990;78(2):204–217.
60. Folch J, Lees M, Sloane Stanley GH. A simple method for the isolation and purification of total lipides from animal tissues. *J Biol Chem*. 1957;226(1):497–509.
61. Mackay AM, Beck SC, Murphy JM, Barry FP, Chichester CO, Pittenger MF. Chondrogenic differentiation of cultured human mesenchymal stem cells from marrow. *Tissue Eng*. 1998;4(4):415–428.
62. Erben RG. Embedding of bone samples in methylmethacrylate: an improved method suitable for bone histomorphometry, histochemistry, and immunohistochemistry. *J Histochem Cytochem*. 1997;45(2):307–313.